Formation of the Conducting Filament in TaO_x-Resistive Switching Devices by Thermal-Gradient-Induced Cation Accumulation

Yuanzhi Ma[1], Dasheng Li[1], Andrew A. Herzing[2], David A. Cullen[3], Brian T. Sneed[3], Karren. L. More[3], N. T. Nuhfer[1], James A. Bain[4], and Marek Skowronski[1]*

[1] Dept. Materials Science and Engineering, Carnegie Mellon University, Pittsburgh, PA 15213
[2] National Institute of Standards and Technology, Gaithersburg, MD 20899
[3] Oak Ridge National Laboratory, Oak Ridge, TN 37831
[4] Dept. Electrical and Computer Engineering, Carnegie Mellon University, Pittsburgh, PA 15213

Abstract

The distribution of tantalum and oxygen ions in electroformed and/or switched TaO_x-based resistive switching devices has been assessed by high-angle annular dark-field microscopy, X-ray energy-dispersive spectroscopy, and electron energy-loss spectroscopy. The experiments have been performed in the plan-view geometry on the cross-bar devices producing elemental distribution maps in the direction perpendicular to the electric field. The maps revealed an accumulation of +20% Ta in the inner part of the filament with a 3.5% Ta-depleted ring around it. The diameter of the entire structure was approximately 100 nm. The distribution of oxygen was uniform with changes, if any, below the detection limit of 5%. We interpret the elemental segregation as due to diffusion driven by the temperature gradient, which in turn is induced by the spontaneous current constriction associated with the negative differential resistance-type I-V characteristics of the as-fabricated metal/oxide/metal structures. A finite-element model was used to evaluate the distribution of temperature in the devices and correlated with the elemental maps. In addition, a fine-scale (~5 nm) intensity contrast was observed within the filament and interpreted as due phase separation of the functional oxide in the two-phase composition region. Understanding the temperature-gradient-induced phenomena is central to the engineering of oxide memory cells.

Keywords: *Resistive switching, Filament, Soret effect, TEM, XEDS, Modeling*

Introduction

Recent interest in nonvolatile solid state memories has focused on devices based on dielectric oxides such as TaO_x and HfO_x.[1,2] The as-fabricated metal/oxide/metal structures typically exhibit high resistance and need to be conditioned by one-time application of bias that leads to the formation of a permanent small-diameter conducting filament within a resistive oxide film. The process is referred to as "formation" or "electroformation".[3] Clearly, formation is critical for functioning of the switching devices as it determines the switching characteristics including ON and OFF resistances, diameter of the filament, and its composition. In TaO_x and HfO_x with inert electrodes, the formation is interpreted as due to the motion of ions driven by the electric field. Specifically, the field induces oxygen ions to cross the interface with the anode leaving oxygen vacancies in the functional layer.[3,4] Local accumulation of vacancies converts the material to n-type creating a conducting filament which connects both electrodes. Subsequent applications of voltage cause redistribution of vacancies and thereby a change of device resistance *i.e.* switching. Despite being adopted and tested by many groups, the model is not quantitative and is not able to predict the fundamental attributes of the filament such as size, composition, conductivity, and

stability with cycling. In particular, the stability under repeated cycling indicates the presence of forces other than the electric field: mobile oxygen vacancies present in high densities should diffuse out of the filament driven by the concentration gradient, and the filament should dissolve after a few switching cycles.

The above model, referred to as Valence Change Mechanism (VCM), has been investigated by analytical imaging techniques seeking direct evidence of the filament formation. A number of groups reported structural changes in VCM devices observed by transmission electron microscopy and x-ray spectromicroscopy. The estimates of the affected area size, structure, and composition are widely scattered even for devices based on related amorphous binary TiO_x, TaO_x, and HfO_x oxides which are likely to operate with the same mechanism. For example, it is generally accepted that the devices reach high temperatures during switching that could result in the crystallization of the oxide. The size of the crystallized area was reported to be as large as the entire 5x5 μm cross-bar area [5] or as small as 10 nm diameter spot.[6] The size difference could be due to the high (300 μW) versus low (50 μW) dissipated power and low thermal conductance of the structure deposited on a thin electron transparent membrane. Many of the analyzed devices were formed/switched while dissipating more than 5 mW.[7-14] The change of dissipated power by a factor of 100 corresponds to the increase of local temperature by the same factor (assuming the same thermal resistance). One could, therefore, expect not only a quantitatively different behavior, but altogether different phenomena taking place with the effects not relevant to the device technology or to the intrinsic features of the switching process. For example, resistive switching devices sometimes exhibit changes of the top electrode morphology (formation of bubbles or craters).[7,15,16] A number of research groups have eliminated such features by limiting the current during formation and/or switching.[17,19] The changes of the top electrode morphology are not an intrinsic feature of switching but are likely a consequence of high current compliance and/or capacitive discharge.[20,21] It should be noted that the craters frequently were used to identify the location from which the transmission electron microscopy (TEM) samples were prepared. For the results to be relevant to the device technology, the power dissipation should be limited to below 100 μW in devices that are well heat-sunk.

As oxygen is known to be mobile in oxides at relatively low temperatures and its deficiency in many oxides leads to an increase of electrical conductivity, many studies focused on the changes of functional layer stoichiometry: [O]/[Me], where Me is the metal fraction. The evidence of the filament containing suboxides was obtained by electron diffraction and X-ray absorption spectroscopy.[5,22,24] The first of the two detected the diffraction pattern of the Magneli phases with the composition of Ti_nO_{2n-1}. The other detected the presence of the Ti^{3+} absorption spectrum which was interpreted as due to the extra electrons produced by the oxygen deficiency. Both results have been interpreted as due to the oxygen ions leaving the filament either because of the electric field forcing the ions into the metal electrodes or the temperature gradient resulting in the lateral out-diffusion of oxygen.[14,19] However, a local high [O]/[Me] ratio within the filament can be produced by the accumulation of metal ions just as well. It is known that the dominant metal-related defects in oxides are the metal interstitials, which have a diffusion coefficient comparable to that of the oxygen vacancies.[25] These defects are charged, can drift in the electric field, and can be exchanged with the electrodes leading to the local O-deficient oxide.[13] Additional data on local composition have been obtained by electron energy-loss spectroscopy (EELS)[11,13,26,28] and X-ray energy-dispersive spectroscopy (XEDS)[29] and the results have been interpreted in a similar fashion. These results are discussed in more detail together with results obtained in this work.

Recently, it has been suggested that, in addition to the ion motion along the applied electrical bias, the local deviation from stoichiometry can be produced by the lateral motion of ions because of the temperature gradient (Soret effect). [14,30] The experimental evidence for this effect in resistive

switching devices is scarce.[14,19] Kumar *et al*. have performed the elemental analysis by X-ray spectromicroscopy on devices fabricated on thin Si_3N_4 membranes with the beam perpendicular to the 2×2 μm device structure. This geometry allowed for the mapping of X-ray transmission at the wavelength corresponding to the O K-edge. The devices were electroformed and switched hundreds or millions of times using high voltage (5V) and large current (estimated at >1mA). The transmission maps exhibited a number (>10) of bright and dark spots and several dark rings with a bright center. The dark rings were attributed to oxygen depletion at the center of the filament and its accumulation in the lateral ring around it. The redistribution is caused by the temperature gradient driving the oxygen atoms away from the hot center of the filament (Soret effect).

In general, the oxygen-poor filament can form by any combination of either Ta or O migrating in a direction parallel or perpendicular to the applied bias. The bias polarity dependence of SET and RESET processes in bipolar switching devices is a strong indication that the motion along the field is essential for switching. This, however, does not exclude the motion of either type of ions in the perpendicular direction.

In this report, we present the TEM analysis of physical changes in the functional layer of TaO_x-based devices induced by the electroformation process, which were formed with a dissipated power below 50 μW and which are free from the artifacts of excessive heating. We argue that the first step in the electroformation is a thermal runaway leading to spontaneous current constriction and appearance of a small hot spot. This process is referred to as threshold switching and is volatile i.e. does not induce any physical changes in the device structure. Only after long pulse, the diffusion will lead to the permanent changes. The analytical TEM experiments have been performed in the plan-view geometry to monitor the lateral redistribution of ions. We have detected the local accumulation of metal with the metal-poor ring around it, providing a strong evidence of the metal-ion transport via the Soret effect. This observation does not exclude the possibility of the vertical motion of either oxygen or tantalum as the geometry employed did not allow for the observation of motion along the direction of the electric field.

Results and Discussion

The investigated devices have relatively thick functional layers, which typically require high forming and switching voltages.[31,32] This effect was alleviated by lowering the resistivity of the material through reduction of the oxygen partial pressure during deposition of the functional layer. The forming voltage was around 10 V for all devices examined in this report and all exhibited stable memory switching characteristics (example of switching *I-V* is shown in Figure M1). Devices were formed and/or switched using a circuit with the 1 MΩ load resistor connected in series with the device and the voltage source (all *I-V*'s are plotted as a function of voltage across the device, not source voltage). This limited the current during the rapid changes of device resistance to 20 μA - 60 μA.[17]

The methodology used in this report relied on TEM imaging and spectroscopy as have several other studies.[11,26,27] However, two aspects of our experimental approach made it possible to reveal unreported structural characteristics of the filaments. First, the imaging was done in plan-view (*i.e.* with the electron beam parallel to both the direction of current flow and the filament length) on devices with relatively thick TaO_x layers (120 nm). This geometry maximizes the interaction length between the beam and the filament and increases signal to noise ratio for all imaging modalities compared with a cross-sectional view. Contrast was further enhanced by removing the top and bottom electrodes (TiN) and the SiO_2/Si substrate, leaving only the functional layer in the beam path. We have been able to examine the entire region of the functional

oxide in 300 nm × 400 nm cross-bar devices, which is clearly not possible in cross-sectional specimens. This geometry allows only for the elemental mapping of the lateral distributions. Accordingly, we comment only on the lateral motion mechanisms leaving the motion along the direction of the field for other studies. Secondly, the composition of the various layers employed more readily lends itself to characterization via the high-angle annular dark-field (HAADF) imaging mode. HAADF images are obtained by collecting electrons scattered at high angles by Rutherford scattering, which increases rapidly with the atomic number.[33] Since atomic number of Ta is 73 while that of other elements present in the device is much lower (N:14; O:16; Ti:22), the intensity of the collected HAADF images was high and was mostly determined by the local tantalum content.

A low magnification, plan-view HAADF image of a device after formation and 10 switching cycles (forming current of 22 μA) is shown in Figure 1(a). All electrical testing was performed on-chip to assure good heat sinking of the device and preventing excessive temperature excursions expected in the thin STEM samples. The device was in the low resistance state of the memory switch. However, we have also tested devices just after forming and after forming and memory switching stopping at the high resistance state. We have not noticed any significant differences in the atomic distribution in the filament. Apparently, the changes detected in plan-view geometry have been created during electroformation and not affected by subsequent memory switching. This would require mapping out the filament in cross-sectional geometry.

The overlaid dashed lines in Figure 1(a) indicate the positions of the electrode edges in the cross-bar structure. The contrast within the active device area is uniform with the exception of a bright, circular region close to the top edge. Closer inspection also reveals a larger, low intensity ring around the high intensity core (Figure 1(b)). A single feature of this type was observed in every one of the seven electroformed and/or switched devices examined while it was not present in control as-fabricated sample. Accordingly, we attribute this contrast to the filament formation. None of the imaged devices displayed any additional contrast that could be interpreted as due to multiple and/or partial filaments. This is in agreement with results of multiple groups indicating formation of only one filament.[4,5,23,34,35]

Figure 1(b) shows a higher-magnification image of the filament. The diameter of the bright core of the filament is ≈ 65 nm while that of the dark ring is ≈ 110 nm. In addition to these features, both the core and ring show finer scale intensity changes. In the core, the lateral size of these features is ≈ (5 – 8) nm with size decreasing toward the periphery. The sample thickness is uniform within the active device region due to the sample preparation method with both sides polished by Ga beam. The contrast in the vicinity of the filament is, therefore, due to increased high-angle scattering. The intensity changes imply that the core of the filament has increased Ta content while the ring is depleted of Ta compared to the initial film composition. The contrast in Fig. 1(b) was quantified by rotationally averaging the HAADF intensity (normalized by the number of pixels) around the center of the filament region (black line in Figure 1(c)). Close to the center of the filament, the distribution shows large variations because of the fine-scale contrast and small integration volume. The smoothed average is shown as the red dashed line with the black dashed line denoting the average signal intensity away from the filament. The HAADF intensity in the filament core is approximately 20±5% higher than that in the unaffected oxide material far from the core and ring regions. The intensity in the dark ring is approximately 2.5±0.7 % lower than the matrix. The local variations of signal intensity in the filament core are higher and range from 85 % to 140 % of the background intensity. Somewhat similar observations. albeit with lower spatial resolution, have been reported by other groups. Wei *et al*. has observed a dark feature in cross-sectional bright field image of TaO_x switching device[26] Since bright field and HAADF modes typically show reversed contrast compared to bright field, this should also be interpreted as the

local increase of Ta content. Similarly, Strachan *et al*. detected a local increase of the Ta signal in the plan-view map of x-ray fluorescence.[22] Neither group commented on the origin of the contrast.

It is important to note here that the techniques such as bright and dark field TEM or X-ray fluorescence monitor total number of atoms interacting with the beam rather than the ratio of Ta/O as is the case for spectroscopy methods. Local increase of HAADF (as well as XEDS and EELS) intensity, indicates larger number of Ta ions in the TEM sample. We would also like to assert that, since that the sample thickness was uniform and the device surface remained flat as verified by Atomic Force Microscopy, the total number of Ta ions increased at the location of the filament. This can only be explained if Ta ions are mobile during electroforming/switching and accumulate within the filament. This possibility was not considered in most of the existing models of the resistive switching[36-42] even though the formation energies of metal interstitials[25] and their mobility are well documented[25,43,44] and are comparable to those of oxygen. More recent data do indeed indicate that Ta is mobile and electrochemically active in resistive switching devices.[45,46]

In addition to the Ta mobility, the HAADF images indicate that the Ta ions move laterally from the area of the ring to the filament core. Since this flux of Ta is perpendicular to the electric field and occurs in the material with the uniform initial composition, it cannot be driven by the electric field or the composition gradient.

Outside the filament, one can discern a pattern of dark wavy lines. The origin of these features is not clear at this time, but they do not correlate with the electrical testing as they are observed in as-fabricated devices as well (Supporting Information). In addition, they are not due to grain boundaries as the functional layer was amorphous as verified by electron diffraction.

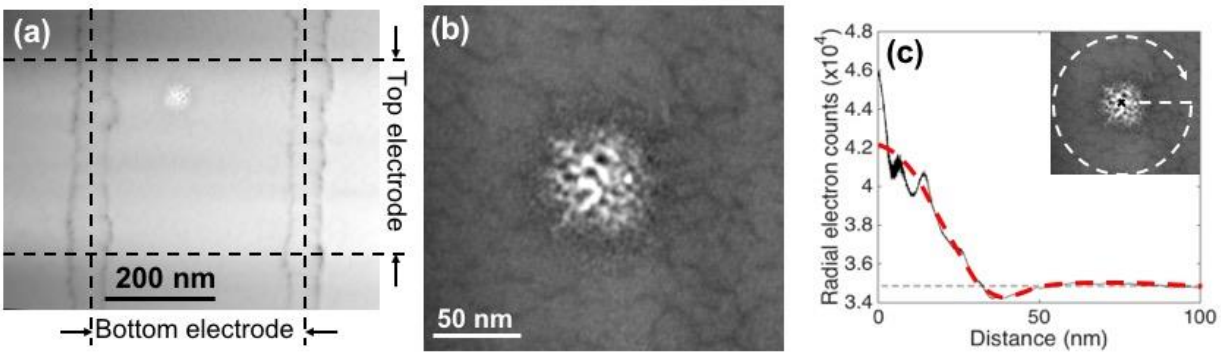

Figure 1. (a) Low magnification plan-view high-angle annular dark-field (HAADF) image of the active area of the TaO_x device. (b) High magnification HAADF image of the filament region. (c) Rotationally averaged HAADF line profile normalized by the number of pixels. The red dotted line indicates a smoothed profile.

The elemental distribution of Ta and O in the formed and switched devices was imaged using XEDS and EELS. The image in Figure 2(a) is the HAADF plan-view image of the filament area in a sample that was only electroformed and serves as a reference (There were no significant differences in any of the maps or spectra obtained from devices that were only formed and those that were formed and switched. Typical forming and switching *I-V* curves are shown in Figure 4(a) and S1 in the Supporting Information). The two examples of XEDS spectra are collected on bright spot in the core of the filament and the background away from it (shown in Fig. 2(b) as red and blue traces). The spectra show only peaks associated with Ta and O emission which is expected

as the electrodes have been removed in the sample preparation process. The intensity of Ta M-line collected on a brightest spot within the filament is about 1.8 times as intense as the corresponding line collected away from the filament. The intensity of the oxygen K-line from the same spot is significantly lower than that in the surrounding area. This result suggests increase of Ta content in agreement with the HAADF images and concomitant oxygen depletion. It is, however, difficult to quantify the concentration of oxygen as the O K-line is strongly absorbed by tantalum. Since the density of Ta is higher within the filament, the apparent decrease of O X-ray emission could be due to increased reabsorption. As a consequence, we have refrained from interpreting the XEDS oxygen intensity distribution maps. Table 1 lists the photon counts obtained on different locations within the filament including bright and dark spots within a core, Ta-depleted ring, and background. The values have been averaged over many locations and are in general agreement with the line profile in Figure 2 (c).

Table 1. Intensities of Ta-M and O-K lines at different locations in the filament.

Location	$I_{Ta\text{-}M\alpha}$ (counts)	$I_{O\text{-}K}$ (counts)
Core (bright spots)	2636	453
Core (dark spots)	1886	488
Ring	1922	510
Background	1988	506

The Ta XEDS M-line does not suffer from the absorption effect and was used to map the Ta distribution shown in Figure 2(c). The map shows one-to-one correlation with HAADF intensity, which confirms attribution of the HAADF contrast to the Ta density changes. The filament region exhibits higher Ta concentration with the local increase by $\approx 20 \pm 5$ % compared with the background (Figure 2(d)). This value corresponds to the concentration change averaged through the sample thickness and is likely much smaller than the local changes associated with the fine structure. A darker ring around the bright core corresponds to $\approx 3.5 \pm 0.7$ % decrease of X-ray intensity. This value has a relatively large error due to changing thickness of the sample close to the ring area. Even though the ring area is bigger than the central core, the integrated HAADF and XEDS signals give positive values corresponding to the net increase of Ta in the oxide. We believe that this effect is due to possible error in background subtraction and the fact that the thickness of the TEM sample was approximately 50 nm and was less than half of the entire functional layer thickness. Potentially, a vertical motion of ions could produce such an increase in the total Ta content in the specimen. Another possible contribution could come from the thin Ta layer that was part of the top electrode. Given a small thickness of this layer (2 nm) compared to the functional layer thickness (120 nm) it appears unlikely that the Ta layer could affect Ta content in the filament more than 5%.

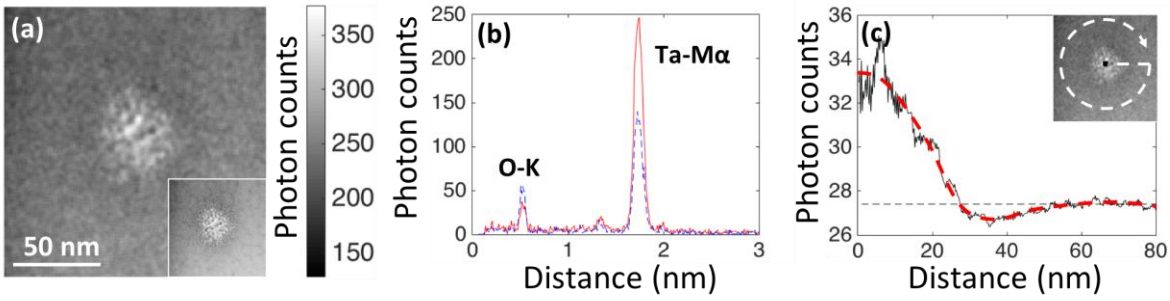

Figure 2 (a) XEDS map of Ta M line intensity (insert shows a reference HAADF image of the same area) (b) Examples of XEDS spectra obtained on bright HAADF spot in the core of the filament (red continuous line) and that of background (dashed blue line). (c) Radially averaged line profile extracted from (a). The red dashed line indicates the smoothed-out profile, the black dashed line is the background intensity, and the inset shows the schematics for averaging.

The oxygen distribution was assessed by EELS on a different sample than the two shown in Figures 1 and 2. The device was electroformed and switched 10 times. Figures 3(a) and (b) show the reference HAADF map of the filament and the two EELS O edge-K spectra collected within (red) and away (blue) from the filament, respectively. There is a clear difference in intensity of the oxygen signal suggesting lower oxygen content within the filament. The oxygen distribution map created using these data shown in Figure 3(c). However, the raw electron count in EELS needs to be corrected for the changes of the beam intensity. In EELS, electrons are collected only within the small aperture around the optical axis of the instrument. In the regions with higher Ta concentration, part of the beam is scattered at high angles missing the detector and effectively lowering the beam intensity. The change of beam intensity was determined by collecting the zero-energy-loss peak intensity map at the same time as the EELS oxygen map. The results are shown in Figure 3(c). The zero-loss-peak map shows a clear decrease of intensity within the filament, similar to that seen in bright field images (not shown) and inverse of that in HAADF. The corrected map of oxygen distribution (Figure 3(d)) is uniform with the precision of experimental error with no indication of depletion of oxygen reported by others. This apparent contradiction warrants a more detailed discussion. The oxygen EELS maps reported so far have not been corrected even though the authors reported the change of the beam intensity in the bright field image.[11,26] It is possible, that the reported oxygen depletion was an experimental artifact. The changes of oxygen distribution reported by Kumar *et al.*[14,19] have occurred only after prolonged switching with high power dissipation. These authors have not reported any changes of oxygen distribution after forming performed in conditions similar to ours. In this respect, the two results are in agreement. A more significant potential issue is that the local increase of one element could lead to large increase of strain energy unless compensated by the decrease of other element density. In other words, there has to be a local depletion of oxygen to allow for extra Ta ions in the sample with uniform thickness. For the sake of discussion, let us assume that there is no strain caused by the Ta accumulation and the starting composition of the oxide is TaO_2. In such material, Ta occupies less than 8% of the volume due to large difference in ionic radii difference between Ta^{4+} and O^{2-}.[47] Increase of Ta ion density by 20% in a unit volume, can be compensated by about 2% decrease of oxygen. Since the experimental error of oxygen content in our EELS maps is 5% we should not be able to detect the oxygen density change induced by the Ta increase. It should be noted here that changing composition of the oxide does not have to cause appearance of uncompensated charges. It is safe to assume that oxygen is always in the O^{2-} state. The charge of the tantalum ions, however, is likely changing with composition. In Ta_2O_5, it is 5+ while in TaO_2 only 4+ always resulting in electrically neutral oxide. The above does not imply that there is no change at all of the oxygen content within the filament compared to that of the initial film composition. Oxygen density could be somewhat smaller that that of the matrix, but the relative change of oxygen atomic density is certainly much smaller than that of tantalum.

The corrections of XEDS and EELS maps to account for re-absorption of X-rays and high-angle scattering by heavy metal ions are clearly significant at least in our experimental conditions. The amount of correction can change depending on thickness of the functional layer and the elemental composition but these effects need to be carefully assessed before reaching conclusions on the relative changes of composition.

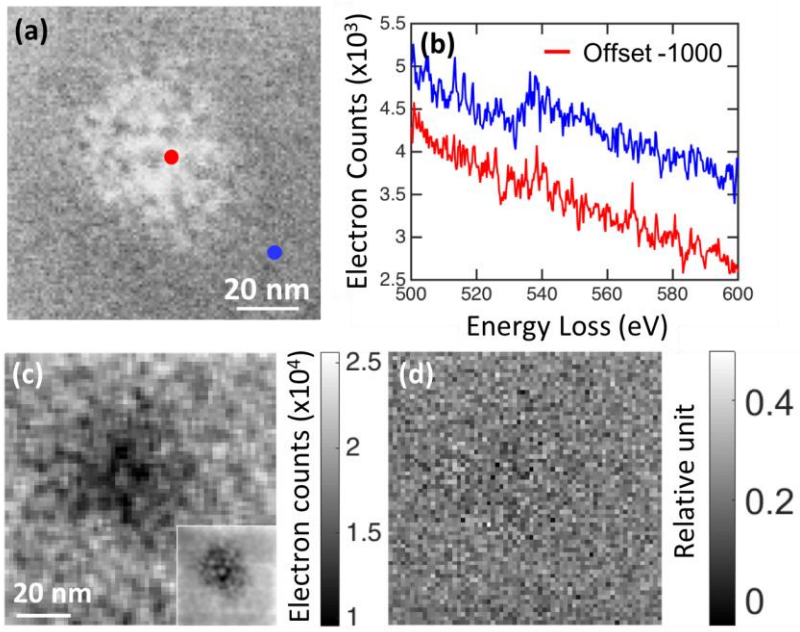

Figure 3. (a) High-angle annular dark-field image of the filament with marked locations where the EELS spectra were collected (b) EELS spectra obtained at red and blue dots in (a), (c) Map of O-K edge intensity. The inset shows the corresponding zero-loss image. (d) Map of O-K edge in (c) normalized by the zero-loss map.

The experimental results above can be summarized as follows. Devices that have been formed/switched at low dissipated power (~50 μW), do not exhibit any electrode morphology changes due to excessive local heating. They do show one well-defined filament with increased Ta content in the center of the filament and a metal-depleted ring around it. The lateral relative oxygen density changes were too small to be detected by EELS. Also, the inside of the filament exhibits a fine-scale contrast also associated with the local changes of Ta content.

The interpretation of electroformation and observed local changes of oxide composition relies on a two-step process similar to that proposed by Strukov *et al*.[30] These authors proposed that, in the first step, a small hot spot is created in the device by any number of mechanisms. This is followed by Soret effect which drives oxygen ions away from the hot spot and produces lasting changes of composition.

We will start the discussion with the step one: formation of the small hot spot in what is initially a uniform device. Typically as-fabricated metal/oxide/metal devices exhibit current that increases superlinearly with applied voltage. The $\partial I/\partial V$ is increasing with bias and at threshold voltage becomes infinite. In the circuit that has a large load resistor, the device can enter into part of characteristics where the slope becomes negative (Negative Differential Resistance (NDR) range, see detailed discussion of *I-V* characteristics of unformed TaO_x devices in Sharma *et al.*[48] and Goodwill *et al*.[49]). In addition to TaO_x, the NDR characteristics have been observed in TiO_x[48], VO_x[50] and formed NbO_x.[51] The prevailing model of such behavior relies on fast increase of conductivity with device temperature.[49,51,52] Within NDR region, the current flow is no longer uniform across the device. Instead, the current spontaneously collapses to a narrow constriction and creates a hot spot due to Joule heating.[53] After the bias is removed, the constriction

disappears leaving no physical changes, the device retains its original characteristics. The size of current constriction is not well documented experimentally but in case of TaO_x, we have at our disposal an electrothermal model that is able to reproduce the experimental *I-V* characteristics and dynamics of switching.[49,54] The model predicts the size of the constriction in the 0.1-1.0 μm range, depending on the composition of the functional layer, and the temperatures exceeding 1000K.[49] The model is used here to estimate the current density distribution and the temperature in structures used in the TEM experiments described above.

The forming experiments have been conducted using a circuit consisting of a voltage source, a switching device and a series resistor with $R_S = 10^6$ Ohm with the experimental *I-V* shown as black line in Figure 4(a). As described above, the *I-V* characteristics exhibit NDR region in which the current spontaneously constricts.[49] If the voltage sweep is stopped soon after the knee (the point at which $\partial I/\partial V$ becomes infinite), the device can return to its initial state if the bias is removed. With further increase of source voltage (the voltage across the device used in Fig. 4(a) is dropping), current constricts further and, at some point, the device threshold switches and transitions along the load line (black dashed line) to a new state with even smaller and hotter constriction.[49] Almost immediately afterwards, the device electroforms permanently changing its characteristics: the return trace of the characteristics (upper branch of the *I-V*) differs from the initial one (Sharma *et al*. Fig. 4).[48]

The experimental threshold switching *I-V* in Fig. 4(a) was simulated using a finite element model, which solved two coupled differential equations describing charge and heat flow. The results are shown as blue squares (detailed description can be found in Supporting Information). The model reproduced the main features of the experimental *I-V* with correct value of the knee voltage and the switching event without any adjustable parameters such as the size of constriction or conductivity. In parallel, this approach produced the current density (Fig. 4(b)) and temperature distribution (Fig. 4(c)) in the device. As is apparent from Figure 4(b), the limit imposed by the load resistor on the current in the forming circuit led to the current constriction with the current forming a cone with the tip near the bottom electrode and the wider base at the top. The shape of the constriction is caused by the larger than typical thickness of the functional oxide. In thinner oxides, the current density distribution has more cylindrical shape with the maximum temperature in the middle of the oxide. For the device structure investigated here, the maximum of temperature is shifted toward the bottom electrode. It is evident that the steepest temperature gradient is oriented laterally with a smaller but still significant component pointing vertically toward the bottom electrode. The upper range of simulated temperatures (>1000K) has significant uncertainty as the values of electrical and thermal conductivities of materials used in the device structure are not well known in this temperature range. The transition from the OFF to ON states of the threshold switch takes less than 10 ns, a time that does not allow for appreciable diffusion distance.[54] One can, therefore, approximate the entire forming process by two distinct steps. First, the device quickly forms the hot spot during threshold switching event, which is followed by slower diffusion of ions in the imposed temperature distribution.

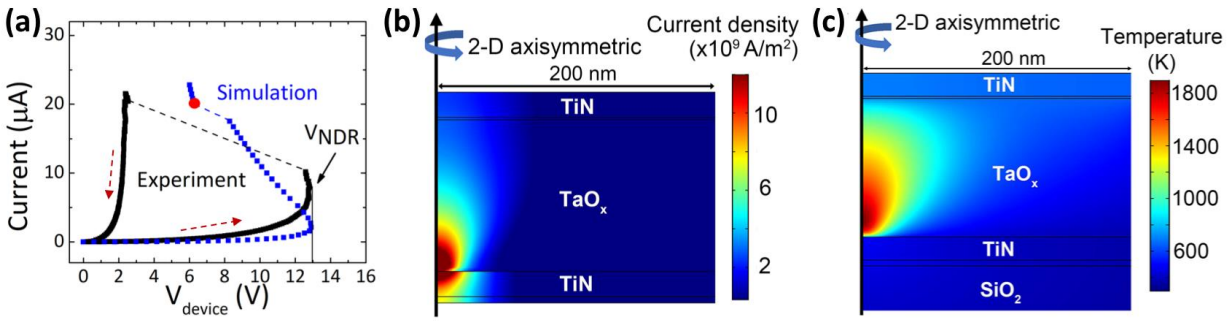

Figure 4. (a) Experimental (black squares) and simulated (blue squares) forming *I-V* of the device. Simulated current density (b) and temperature distribution (c) right after the threshold switch (red point in (a)).

The segregation of oxygen and tantalum in the TaO_x functional layer somewhat resembles elemental segregation in phase change threshold and memory devices.[55] The driving forces that have been proposed in this case include carrier wind, the electric field, the temperature gradient (Soret effect), the mechanical stress induced by the local lattice expansion, and the instability of the oxide.[55,56] The last of these forces originates from the fact that there are only two stable phases in the Ta-O binary system: Ta and $TaO_{2.5}$.[57] The starting composition in our devices [O]/[Ta] is between 2 and 2.5 based on XEDS and atom probe tomography measurements (data not included). Under prolonged heating, the functional layer should separate into these two crystalline phases. In switching experiments, the high temperature was not maintained long enough to cause complete segregation and crystallization, but one could expect partial segregation. Among the five segregation phenomena listed above, the first two could only induce vertical motion of ions, which could not be detected in plan-view geometry. The same applies to the compressive stress induced by thermal expansion: lateral motion of ions could not relieve the accumulated strain energy. In any event, the change of lattice parameter between room temperature and 1000K is only 0.4%[58] and could only induce a comparable amount of atom density change. This leaves only the last two to account for the observed concentration profiles. Once the segregation produces concentration differences, another driving force, the concentration gradient, would act as the opposing agent trying to homogenize the oxide. The balance between these forces would lead to steady state distribution.

The segregation driven by the temperature gradient has to produce the distribution with the symmetry reflecting that of the driving force. Among the two segregation length scales, the large scale corresponds to the accumulation of Ta in the center of the filament as well as the depletion of Ta in the ring, and the fine scale corresponds to the blotched contrast throughout the feature. It is the large scale segregation that has the required symmetry. The large-scale Ta density profile in Figure 2(d) could be interpreted as follows. The lateral flux of Ta or O ions because of the Soret effect is given by:

$$j_k = c_k D_k S_k \nabla T \qquad (1)$$

Where the subscript *k* corresponds to the component k, *c* is the molar concentration, *D* is the isothermal diffusion coefficient, S is Soret coefficient, and ∇T is the temperature gradient. The sign of S_{Ta} is positive and the flux is directed toward the center of the constriction. Far from the constriction, the diffusion coefficient D_{Ta} is very low and the flux is close to zero. As one moves toward the hot spot, the flux is increasing monotonically with temperature. For a given volume between distance r from the center and r+Δr, the flux from the outside of the ring is lower than the flux out toward the center. This creates a locally Ta depleted region at the periphery of the hot spot. At certain distance from the center, the flux reaches maximum and gradually decreases to zero at the center. Using the temperature distribution shown in Figure 4(b) and the values of Ta diffusion coefficient, one can estimate the size of the permanent filament. We have assumed that one can detect the changes in the composition of the film if the mean square displacement due to diffusion during 10 ms at the simulated temperature is equal to 1 nm. This gives the value of the Ta diffusion coefficient of 5×10^{-17} m^2/s. Unfortunately the values of Ta diffusion coefficient in amorphous TaO_2 is not known and we have used the value determined by Gries *et al*. for the diffusion of Nb in crystalline Ta_2O_5.[59] This gave the temperature at the outer boundary of the filament of ~1000K. The map of the radial temperature distribution in the constriction in the plane

parallel to and 80 nm above the bottom electrode interface is shown in Figure 5(a). This particular distance was selected as the sample used in STEM experiments was likely located in the upper part of the device. The diameter of the circle corresponding to 1000K is approximately 80 nm and this would be the estimated diameter of the outer Ta-depleted ring. The diameter observed in the HAADF image was 110 nm.and well within a factor of two of the estimate.

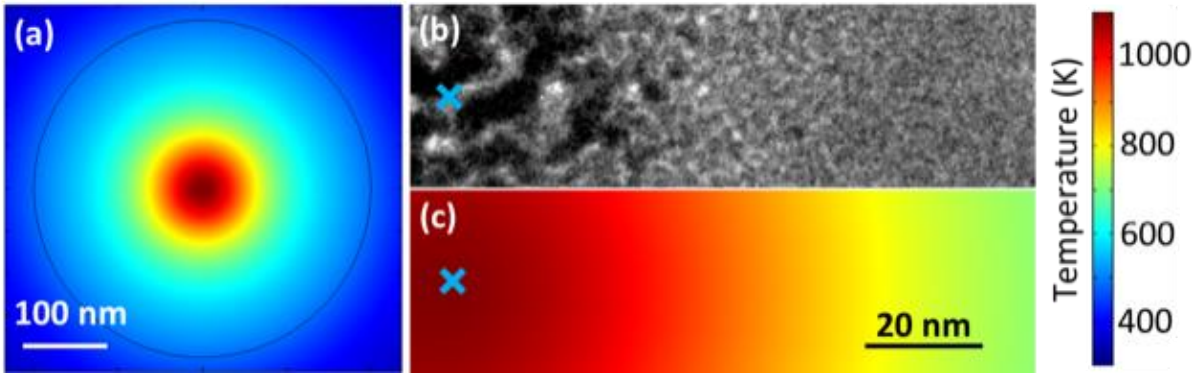

Figure 5. (a) Modeled plan-view temperature distribution during threshold switching in a plane 80 nm above the interface between TaO_x functional layer and bottom electrode. The black circle is the boundary of the active device region. (b) Cropped bright-field image of the filament and surrounding region (blue cross marks the center of the). (c) Corresponding temperature distribution in the same area as (b).

The direction of Ta motion reported here is opposite to that of oxygen suggested by others. It is of interest to explore the origin of such difference. The Soret coefficient for atomic transport because of the motion of vacancies is given by:[60]

$$S_V = \frac{q^*_V - h_V}{kT^2} \qquad (2)$$

where q^*_V is the heat of transport and h_V is the activation enthalpy of motion (of a vacancy). In their derivation, Strukov *et al*. have neglected the heat of transport term[30] and concluded that the Soret coefficient in equation (1) for oxygen should be negative. This would result in oxygen diffusing away from the hot center of the constriction. The transport of Ta is due to the motion of interstitials, and the corresponding formula for the Soret coefficient is:

$$S_I = \frac{q^*_I + h_I}{kT^2} \qquad (3)$$

If one neglects the q^*, the flux would be opposite to that oxygen, i.e. the temperature gradient would drive tantalum ions toward the high temperatures in agreement with the experiment. It should be noted, however, that the absolute value of the heat of transport can be higher than the enthalpy and can be of either sign. At this point in time, there is no available model of the heat of transport and we cannot predict the sign of the Soret coefficient. Its values are typically determined from experiment and have been found be either positive or negative. For example, the magnitude of the Soret coefficients for Ge and Sb in $Ge_2Sb_2Te_5$ have opposite sign.[55,56]

The remaining issue is a possible effect of phase separation and the origin of fine contrast in the elemental maps presented above. It is easy to notice that the scale of fine contrast is changing with the temperature at any given location: the size of the bright and dark areas in the center of the filament is about 5 nm and decreases to 1 nm at the distance of 40 nm from the center (Figure 5(b)). The contrast is equiaxial (at least in the plan view presented here): the intensity changes

along the radial direction as well as perpendicular to it. The azimuthal variation cannot be caused by the temperature gradient as it has only radial component. The fine-scale segregation is, in our opinion, due to the decomposition of TaO_x toward the two stable phases in the phase diagram. [57] The change of size is associated with Ostwald coarsening, with the size of the feature increasing with the local temperature (the time at the temperature was approximately the same).

Figure 6 presents a sequence of events proposed here as the mechanism for the electro-formation of conducting filaments in metal oxides. The initial state corresponds to a uniform distribution of Me^{x+} ions and a uniform current flow at low voltages (a). At the threshold voltage, the device threshold switches to the volatile ON state characterized by a small diameter hot constriction with large lateral temperature gradient (b) and a smaller vertical component marked by the red arrows. The gradient produces the flux of Ta ions by the Soret effect (c) and results in accumulation of excess metal in the hot center of the filament (d). It should be noted here that the proposed sequence does not address bipolar switching.

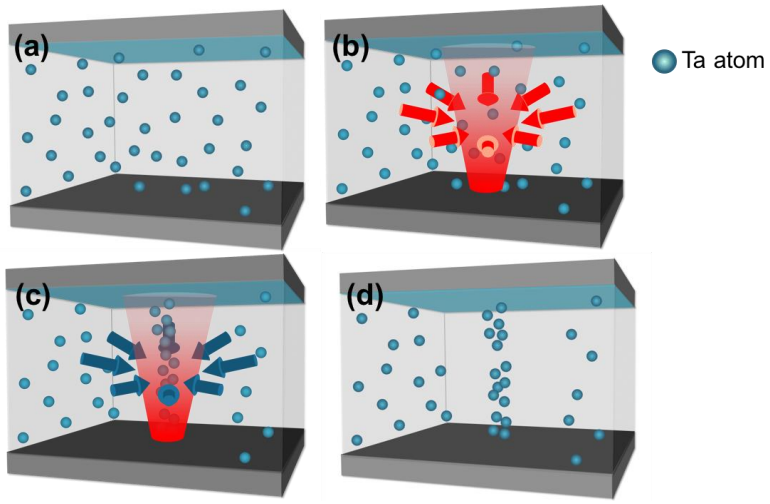

Figure 6. Proposed model for the formation of the conducting filament in TaO_x based RRAM. (a) As deposited uniform distribution of Ta ions in the functional layer. (b) Threshold switching-induced volatile current constriction and the temperature gradient distribution. (c) Ta atoms migrate in the functional oxide. (d) Permanent Ta-rich filament is created as result of the forming event.

As proposed, the process includes two positive feedback loops that could result in runaway events. The first one is the thermal feedback resulting in the threshold switching event. This process can be illustrated by considering the device response to applied voltage pulse. Immediately after the beginning of the pulse, the current reaches value corresponding to the conductivity at the stage temperature. The dissipated Joule heat causes a temperature rise which in oxides results in current increase. If the dependence of electrical conductivity on temperature is steep enough, this positive feedback loop will produce rapid increase of temperature and current. The process will stop whenever the external load or some extraneous process within the device (for example melting and delamination of the electrodes) will limit current increase in the circuit. The size and maximum temperature of the hot spot created by this event is determined mostly by the circuit (load) external to the device rather than by intrinsic device or material characteristics. Since the load is rarely mentioned in reports on resistive switching (current compliance set on the sourcemeter cannot replace the load located next to the device[17]), the temperatures reached during electroformation are not known with any accuracy resulting in a large range of effects observed. In the experiments described above, the load was carefully selected, and its effects

included in the model of temperature distribution.

The second runaway is of chemical nature and is caused by positive feedback between oxide composition and conductivity. As the temperature gradient drives the Ta ions toward the center of the filament, the changing stoichiometry causes an increase of conductivity and total current. This, in turn, increases the temperature and the temperature gradient i.e. the driving force for elemental segregation. In many devices structures/electrical bias scenarios, this can lead to a second runaway event, this time the runaway of composition. The consequences include rapid rather than gradual change of permanent filament resistance[3,61]. It also is expected that the diameter of the cylinder with increased Ta content, would decrease as the result. At the end of the process, one could form a very small metallic Ta filament. Once such a filament forms, the conductivity would become constant with current increasing only with the diameter of the filament. The compositional runaway should stop. It is likely that the process would come to steady state before formation of the metallic Ta phase if the dependence of conductivity on composition levels off at high oxygen deficiencies. The limited available data on conductivity do not allow for making a definitive assessment of the final filament composition. The highest increase of local Ta atomic percent obtained from the XEDS is 80% (assuming the initial composition to be TaO_2). This fraction is almost certainly an underestimate as the composition values are averaged over the thickness of the sample. It could well be that some of the bright spots in the Ta intensity maps correspond to Ta phase. The filament thus created resembles very closely the filaments reported in the conducting bridge memory devices in which the conduction occurs between metallic inclusions created by coalescence of cations.[62-64]

Independently of these arguments and similarly to the thermal runaway, the chemical runaway could also be forced to stop by the current limit imposed by the circuit. This would make the size and composition of the filament very strongly dependent on experimental conditions of forming and switching. Accordingly, these characteristics are not universal and particular values reported here should only be applied to other devices/processes with caution. The value of the results rests in identification of processes and their relative magnitudes.

The significant role played by the Soret effect in electroformation process explains the relative stability of the filament over as many as 10^{12} switching cycles reported in literature.[1] It is clear that the nonvolatile filament gets hot during switching as the power dissipated over small volume of the filament must lead to large temperature excursions.[38,65,66] This has to lead to high diffusion coefficients and atomic fluxes down the concentration gradient. As the consequence, concentration-gradient-induced diffusion would result in dissolution of the filament after a few switching events. Clearly, this does not happen. The Soret flux of Ta toward the core compensates the outward diffusion flux providing for the filament neither shrinking or dissolving. The same argument applies to oxygen and oxygen vacancies. It is also important to note that Soret effect should play an important role in switching in addition to that played in electroformation. The temperature gradients close to interfaces with metallic electrodes are expected to exert a force on the ions driving both oxygen and metal ions in the vertical direction as well as the lateral one. This force should be quantified and included together with electrostatic and carrier wind components in a comprehensive model of resistive switching. Moreover, the fact that Ta segregation induced by the temperature gradient is much more pronounced than that of oxygen could indicate that the same applies to motion induced by the electric field i.e. that the switching is due mostly to the motion of metal ions rather than that of oxygen. Such a hypothesis would require a careful assessment of elemental drift and discussion in cross-sectional geometry.

Experimental Section

Device fabrication. The devices were fabricated on Si substrates covered by 1 μm thick thermal SiO_2 layer. The bottom electrode (400 nm in width) was defined using electron-beam lithography, followed by sputter deposition of 5 nm Ta and 20 nm TiN and the lift-off process. The 120 nm of functional TaO_x was deposited by reactive sputtering using Ta target and a mixture of oxygen (4 sccm) and argon (56 sccm) gas at chamber pressure of 3 mTorr. The 2 nm Ta/20 nm TiN top electrode layer (370 nm in width) was defined by electron-beam lithography and lift-off.

Electrical testing. The devices were tested using a quasi-DC voltage source (Agilent 4155C Semiconductor Parameter Analyzer) with a load resistor of 1 MΩ connected in series with the device. No external current compliance was used. (Any mention of commercial products within this publication is for information only; it does not imply recommendation or endorsement by NIST.) The I-V characteristics of electroformation and resistive switching are shown in supporting information (Figure S1).

Microstructural Analysis. The devices were lifted-out and thinned down by FIB (FEI Helios and FEI NOVA Nanolab 600) and characterized by TEM/STEM. Detailed description of FIB lift-out can be found in supporting information. The HAADF images in Figure 1 were taken using FEI Titan 80-300 operating at 300 keV; the HAADF and XEDS analysis in Figure 2(a) and (b) were performed using FEI Talos F200X at 200 keV. The HAADF images were collected with an angle higher than 50 mrad to ensure exclusive Z-contrast in the images. The EELS O-K map in Figure 2(c) was extracted from EELS spectrum image at 532-572 eV. The EELS spectrum image was taken using Hitachi HF3300 S/TEM operating at 300 keV.

Electrothermal simulation. The heat and charge flow in devices was simulated using COMSOL Multiphysics finite element software package. The device structure was created to reproduce the as-fabricated device (Figure S2). The temperature distribution and electrical conductivity are solutions to coupled equations describing heat flow equation and the three-dimensional Poole-Frankel formula. During the simulation, the temperature of the bottom surface of the Si was fixed at 300 K while the top and side surfaces of the structure were thermally insulated. Electrically, the bottom surface of the bottom electrode was at electrical ground, and the top surface of the top electrode was connected to an outside circuit with 1 MΩ load resistor and the voltage source. The amplitude of the applied source voltage was the same as during electrical testing, which was 22 V with a ramp rate of 4 V/s. It should be noted here that in Fig. 4(a) and S1 current is plotted as a function of device voltage (across the device) while the voltage mentioned here is the source voltage (across the device and the load resistor). A thermal boundary conductance of 100 MW/m^2K was included at the metal / oxide interfaces. The TaO_x sandwiched in between is 120 nm thick. The details of the simulations can be found in Supporting Information.

Associated Content

Supporting Information

The Supporting Information is available free of charge on the ACS Publications website at DOI:

Electrical testing; FIB lamella preparation for TEM analysis; Control experiment on as-fabricated devices; Electrothermal simulation; Figure S1-S3.

AUTHOR INFORMATION

Corresponding author:
*E-mail: mareks@cmu.edu
ORCID:
Marek Skowronski: 0000-0002-2087-0068

Notes:
The authors declare no competing financial interests.

ACKNOWLEDGMENTS

We would like to acknowledge useful discussions with Prof. R. F. Egerton and Dr. J. Kwon. This work was in part supported by FAME, one of six centers of STARnet, a Semiconductor Research Corporation program sponsored by MARCO and DARPA, by NSF Grant DMR 1409068, and Data Storage Systems Center at Carnegie Mellon University. The authors acknowledge use of the Materials Characterization Facility at Carnegie Mellon University supported by grant MCF-677785 and microscopy facilities at Oak Ridge National Laboratory's Center for Nanophase Materials Sciences, which is a U.S. Department of Energy, Office of Science User Facility. EELS data was collected at the Center for Nanophase Materials Sciences, which is a DOE Office of Science User Facility.

REFERENCES

(1) Lee, M. J.; Lee, C. B.; Lee, D.; Lee, S. R.; Chang, M.; Hur, J. H.; Kim, Y. B.; Kim, C. J.; Seo, D. H.; Seo, S.; Chung, U. I.; Yoo, I. K.; Kim, K. A Fast, High-Endurance and Scalable Non-Volatile Memory Device Made From Asymmetric Ta_2O_{5-x}/TaO_{2-x} Bilayer Structures. *Nat. Mater.* **2011**, *10* (8), 625–630.

(2) Yu, S.; Chen, H. Y.; Gao, B.; Kang, J.; Wong, H. S. P. HfO_x-Based Vertical Resistive Switching Random Access Memory Suitable for Bit-Cost-Effective Three-Dimensional Cross-Point Architecture. *ACS Nano* **2013**, *7* (3), 2320–2325.

(3) Jeong, D. S.; Schroeder, H.; Breuer, U.; Waser, R. Characteristic Electroforming Behavior in Pt/TiO2/Pt Resistive Switching Cells Depending on Atmosphere. *J. Appl. Phys.* **2008**, *104* (12), 123716.

(4) Waser, R.; Dittmann, R.; Staikov, G.; Szot, K. Redox-Based Resistive Switching Memories - Nanoionic Mechanisms, Prospects, and Challenges. *Adv. Mater.* **2009**, *21* (25-26), 2632–2663.

(5) Strachan, J. P.; Pickett, M. D.; Yang, J. J.; Aloni, S.; Kilcoyne, A. L. D.; Medeiros-Ribeiro, G.; Williams, R. S. Direct Identification of the Conducting Channels in a Functioning Memristive Device. *Adv. Mater.* **2010**, *22* (32), 3573–3577.

(6) Kwon, J.; Sharma, A. A.; Chen, C. Y.; Fantini, A.; Jurczak, M.; Herzing, A. A.; Bain, J. A.; Picard, Y. N.; Skowronski, M. Transient Thermometry and High-Resolution Transmission Electron Microscopy Analysis of Filamentary Resistive Switches. *ACS Appl. Mater. Interfaces* **2016**, *8* (31), 20176–20184.

(7) Kwon, D. H.; Kim, K. M.; Jang, J. H.; Jeon, J. M.; Lee, M. H.; Kim, G. H.; Li, X. S.; Park, G. S.; Lee, B.; Han, S.; Kim, M.; Hwang, C. S. Atomic Structure of Conducting Nanofilaments in TiO_2 Resistive Switching Memory. *Nat. Nanotechnol.* **2010**, *5* (2), 148–153.

(8) Jeong, H. Y.; Lee, J. Y.; Choi, S. Y. Direct Observation of Microscopic Change Induced by Oxygen Vacancy Drift in Amorphous TiO_2 Thin Films. *Appl. Phys. Lett.* **2010**, *97* (4), 042109.

(9) Kim, K. M.; Song, S. J.; Kim, G. H.; Seok, J. Y.; Lee, M. H.; Yoon, J. H.; Park, J.;

Hwang, C. S. Collective Motion of Conducting Filaments in Pt/n-Type TiO_2/p-Type NiO/Pt Stacked Resistance Switching Memory. *Adv. Funct. Mater.* **2011**, *21* (9), 1587–1592.

(10) Kim, G. H.; Lee, J. H.; Seok, J. Y.; Song, S. J.; Yoon, J. H.; Yoon, K. J.; Lee, M. H.; Kim, K. M.; Lee, H. D.; Ryu, S. W.; Park, T. J.; Hwang, C. S. Improved Endurance of Resistive Switching TiO_2 Thin Film by Hourglass Shaped Magneli Filaments. *Appl. Phys. Lett.* **2011**, *98* (26), 262901.

(11) Miao, F.; Strachan, J. P.; Yang, J. J.; Zhang, M.-X.; Goldfarb, I.; Torrezan, A. C.; Eschbach, P.; Kelley, R. D.; Medeiros-Ribeiro, G.; Williams, R. S. Anatomy of a Nanoscale Conduction Channel Reveals the Mechanism of a High-Performance Memristor. *Adv. Mater.* **2011**, *23* (47), 5633–5640.

(12) Yang, M. K.; Ju, H.; Kim, G. H.; Lee, J. K.; Ryu, H.-C. Direct Evidence on Ta-Metal Phases Igniting Resistive Switching in TaO_x Thin Film. Sci. Rep. **2015**, 5, 1–7.

(13) Jiang, H.; Han, L.; Lin, P.; Wang, Z.; Jang, M. H.; Wu, Q.; Barnell, M.; Yang, J. J.; Xin, H. L.; Xia, Q. Sub-10 Nm Ta Channel Responsible for Superior Performance of a HfO_2 Memristor. *Sci. Rep.* **2016**, *6*, 1–8.

(14) Kumar, S.; Graves, C. E.; Strachan, J. P.; Grafals, E. M.; Kilcoyne, A. L. D.; Tyliszczak, T.; Weker, J. N.; Nishi, Y.; Williams, R. S. Direct Observation of Localized Radial Oxygen Migration in Functioning Tantalum Oxide Memristors. *Adv. Mater.* **2016**, *28* (14), 2772–2776.

(15) Yang, J. J.; Miao, F.; Pickett, M. D.; Ohlberg, D. A. A.; Stewart, D. R.; Lau, C. N.; Williams, R. S. The Mechanism of Electroforming of Metal Oxide Memristive Switches. *Nanotechnol.* **2009**, *20* (21), 215201.

(16) Dittmann, R.; Muenstermann, R.; Krug, I.; Park, D.; Menke, T.; Mayer, J.; Besmehn, A.; Kronast, F.; Schneider, C. M.; Waser, R. Scaling Potential of Local Redox Processes in Memristive $SrTiO_3$ Thin-Film Devices. *Proc. IEEE* **2012**, *100* (6), 1979–1990.

(17) Lu, Y. M.; Noman, M.; Chen, W.; Salvador, P. A.; Bain, J. A.; Skowronski, M. Elimination of High Transient Currents and Electrode Damage During Electroformation of TiO_2-Based Resistive Switching Devices. *J. Phys. D: Appl. Phys.* **2012**, *45* (39), 395101.

(18) Ninomiya, T.; Katayama, K.; Muraoka, S.; Yasuhara, R.; Mikawa, T.; Wei, Z. Conductive Filament Expansion in TaOx Bipolar Resistive Random Access Memory During Pulse Cycling. *Jpn. J. Appl. Phys.* **2013**, *52* (11R), 114201–114205.

(19) Kumar, S.; Wang, Z.; Huang, X.; Kumari, N.; Davila, N.; Strachan, J. P.; Vine, D.; Kilcoyne, A. L. D.; Nishi, Y.; Williams, R. S. Oxygen Migration During Resistance Switching and Failure of Hafnium Oxide Memristors. *Appl. Phys. Lett.* **2017**, *110* (10), 103503–103504.

(20) Kinoshita, K.; Tsunoda, K.; Sato, Y.; Noshiro, H.; Yagaki, S.; Aoki, M.; Sugiyama, Y. Reduction in the Reset Current in a Resistive Random Access Memory Consisting of NiO_x Brought About by Reducing a Parasitic Capacitance. *Appl. Phys. Lett.* **2008**, *93* (3), 033506–4.

(21) Fan, Y. S.; Zhang, L.; Crotti, D.; Witters, T.; Jurczak, M.; Govoreanu, B. Direct Evidence of the Overshoot Suppression in Ta_2O_5-Based Resistive Switching Memory with an Integrated Access Resistor. *IEEE Electron Device Lett.* **2015**, *36*

(10), 1027–1029.
(22) Strachan, J. P.; Medeiros-Ribeiro, G.; Yang, J. J.; Zhang, M.-X.; Miao, F.; Goldfarb, I.; Holt, M.; Rose, V.; Williams, R. S. Spectromicroscopy of Tantalum Oxide Memristors. *Appl. Phys. Lett.* **2011**, *98* (24), 242114.
(23) Strachan, J. P.; Strukov, D. B.; Borghetti, J.; Yang, J. J.; Medeiros-Ribeiro, G.; Williams, R. S. The Switching Location of a Bipolar Memristor: Chemical, Thermal and Structural Mapping. *Nanotechnol.* **2011**, *22* (25), 254015.
(24) Strachan, J. P.; Yang, J. J.; Montoro, L. A.; Ospina, C. A.; Ramirez, A. J.; Kilcoyne, A. L. D.; Medeiros-Ribeiro, G.; Williams, R. S. Characterization of Electroforming-Free Titanium Dioxide Memristors. *Beilstein J. Nanotechnol.* **2013**, *4* (1), 467–473.
(25) Zhu, L.; Zhou, J.; Guo, Z.; Sun, Z. Synergistic Resistive Switching Mechanism of Oxygen Vacancies and Metal Interstitials in Ta_2O_5. *J. Phys. Chem. C* **2016**, *120* (4), 2456–2463.
(26) Wei, Z.; Takagi, T.; Kanzawa, Y.; Katoh, Y.; Ninomiya, T.; Kawai, K.; Muraoka, S.; Mitani, S.; Katayama, K.; Fujii, S.; Miyanaga, R.; Kawashima, Y.; Mikawa, T.; Shimakawa, K.; Aono, K. Demonstration of High-Density ReRAM Ensuring 10-Year Retention at 85ºC Based on a Newly Developed Reliability Model. IEEE Int. Electron Devices Meet. 2011, pp 31.4.1–31.4.4.
(27) Park, G. S.; Kim, Y. B.; Park, S. Y.; Li, X. S.; Heo, S.; Lee, M. J.; Chang, M.; Kwon, J. H.; Kim, M.; Chung, U. I.; Dittmann, R.; Waser, R.; Kim, K. In Situ Observation of Filamentary Conducting Channels in an Asymmetric Ta_2O_{5-x}/TaO_{2-x} Bilayer Structure. *Nat. Commun.* **2013**, *4*, 1–9.
(28) Privitera, S.; Bersuker, G.; Butcher, B.; Kalantarian, A.; Lombardo, S.; Bongiorno, C.; Geer, R.; Gilmer, D. C.; Kirsch, P. D. Microscopy Study of the Conductive Filament in HfO_2 Resistive Switching Memory Devices. *Microelectron. Eng.* **2013**, *109* (C), 75–78.
(29) Yang, Y.; Zhang, X.; Qin, L.; Zeng, Q.; Qiu, X.; Huang, R. Probing Nanoscale Oxygen Ion Motion in Memristive Systems. *Nat. Commun.* **2017**, *8*, 1–10.
(30) Strukov, D. B.; Alibart, F.; Williams, R. S. Thermophoresis/Diffusion as a Plausible Mechanism for Unipolar Resistive Switching in Metal–Oxide–Metal Memristors. *Appl. Phys. A* **2012**, *107* (3), 509–518.
(31) Chen, A. Area and Thickness Scaling of Forming Voltage of Resistive Switching Memories. *IEEE Electron Device Lett.* **2013**, *35* (1), 57–59.
(32) Govoreanu, B.; Kar, G. S.; Chen, Y. Y.; Paraschiv, V.; Kubicek, S.; Fantini, A.; Radu, I. P.; Goux, L.; Clima, S.; Degraeve, R.; Jossart, N.; Richard, O.; Vandeweyer, T.; Seo, K.; Hendrickx, P.; Pourtois, G.; Bender, H.; Altimime, L.; Wouters, D. J.; Kittl, J. A.; Jurczak, M. $10x10nm^2$ Hf/HfO_x Crossbar Resistive RAM with Excellent Performance, Reliability and Low-Energy Operation. IEEE Int. Electron Devices Meet. 2011; pp 31.6.1–31.6.4.
(33) Egerton, R. F. Electron Energy-Loss Spectroscopy in the TEM. *Rep. Prog. Phys.* **2008**, *72* (1), 016502.
(34) Strachan, J. P.; Yang, J. J.; Muenstermann, R.; Scholl, A.; Medeiros-Ribeiro, G.; Stewart, D. R.; Williams, R. S. Structural and Chemical Characterization of TiO_2 Memristive Devices by Spatially-Resolved NEXAFS. *Nanotechnol.* **2009**, *20* (48), 485701.
(35) Chen, J. Y.; Hsin, C. L.; Huang, C. W.; Chiu, C. H.; Huang, Y. T.; Lin, S. J.; Wu,

W. W.; Chen, L. J. Dynamic Evolution of Conducting Nanofilament in Resistive Switching Memories. *Nano Lett.* **2013**, *13* (8), 3671–3677.
(36) Yu, S.; Wong, H. S. P. A Phenomenological Model for the Reset Mechanism of Metal Oxide RRAM. *IEEE Electron Device Lett.* **2010**, *31* (12), 1455–1457.
(37) Degraeve, R.; Fantini, A.; Clima, S.; Govoreanu, B.; Goux, L.; Chen, Y. Y.; Wouters, D. J.; Roussel, P.; Kar, G. S.; Pourtois, G.; Cosemans, S.; Kittl, J. A.; Groeseneken, G.; Jurczak, M.; Altimime, L. Dynamic "Hour Glass" Model for SET and RESET in HfO_2 RRAM. Symp. VLSI Technol., Dig. Tech. Pap. 2012, pp 75–76.
(38) Larentis, S.; Nardi, F.; Balatti, S.; Gilmer, D. C.; Ielmini, D. Resistive Switching by Voltage-Driven Ion Migration in Bipolar RRAM-Part II: Modeling. *IEEE Trans. Electron Devices* **2012**, *59* (9), 2468–2475.
(39) Kim, S.; Kim, S. J.; Kim, K. M.; Lee, S. R.; Chang, M.; Cho, E.; Kim, Y. B.; Kim, C. J.; Chung, U. I.; Yoo, I. K. Physical Electro-Thermal Model of Resistive Switching in Bi-Layered Resistance-Change Memory. *Sci. Rep.* **2013**, *3* (1), 13–16.
(40) Kim, S.; Choi, S.; Lu, W. Comprehensive Physical Model of Dynamic Resistive Switching in an Oxide Memristor. *ACS Nano.* **2014**, *8* (3), 2369–2376.
(41) Xue, K. H.; Traore, B.; Blaise, P.; Fonseca, L. R. C.; Vianello, E.; Molas, G.; De Salvo, B.; Ghibaudo, G.; Magyari-Kope, B.; Nishi, Y. A Combined Ab Initio and Experimental Study on the Nature of Conductive Filaments in $Pt/HfO_2/Pt$ Resistive Random Access Memory. *IEEE Trans. Electron Devices* **2014**, *61* (5), 1394–1402.
(42) Mickel, P. R.; Lohn, A. J.; James, C. D.; Marinella, M. J. Isothermal Switching and Detailed Filament Evolution in Memristive Systems. *Adv. Mater.* **2014**, *26* (26), 4486–4490.
(43) Davies, J. A.; Domeij, B.; Pringle, J. P. S.; Brown, F. The Migration of Metal and Oxygen During Anodic Film Formation. *J. Electrochem. Soc.* **1965**, *112*, 675-680.
(44) Whitton, J. L. The Measurement of Ionic Mobilities in the Anodic Oxides of Tantalum and Zirconium by a Precision Sectioning Technique. *J Electrochem. Soc.* **1968**, *115* (1), 58-61.
(45) Wedig, A.; Luebben, M.; Cho, D. Y.; Moors, M.; Skaja, K.; Rana, V.; Hasegawa, T.; Adepalli, K. K.; Yildiz, B.; Waser, R.; Valov, I. Nanoscale Cation Motion in TaO_x, HfO_x and TiO_x Memristive Systems. *Nature Nanotechnol.* **2016**, *11* (1), 67–74.
(46) Lubben, M.; Karakolis, P.; Ioannou-Sougleridis, V.; Normand, P.; Dimitrakis, P.; Valov, I. Graphene-Modified Interface Controls Transition From VCM to ECM Switching Modes in Ta/TaO_x Based Memristive Devices. *Adv. Mater.* **2015**, *27* (40), 6202–6207.
(47) Shannon, R. Revised Effective Ionic Radii and Systematic Studies of Interatomic Distances in Halides and Chalcogenides. *Acta Crystallogr., Sect. A* **1976**. *32* (5), 751-767.
(48) Sharma, A. A.; Noman, M.; Abdelmoula, M.; Skowronski, M.; Bain, J. A. Electronic Instabilities Leading to Electroformation of Binary Metal Oxide-Based Resistive Switches. *Adv. Funct. Mater.* **2014**, *24*, 5522-5529.
(49) Goodwill, J. M.; Sharma, A. A.; Li, D.; Bain, J. A.; Skowronski, M. Electro-Thermal Model of Threshold Switching in TaO_x-Based Devices. *ACS Appl. Mater. Interfaces* **2017**, *9* (13), 11704–11710.
(50) Radu, I. P.; Govoreanu, B.; Mertens, S.; Shi, X.; Cantoro, M.; Schaekers, M.;

Jurczak, M.; De Gendt, S.; Stesmans, A.; Kittl, J. A.; Heyns, M.; Martens, K. Switching Mechanism in Two-Terminal Vanadium Dioxide Devices. *Nanotechnol.* **2015**, *26* (16), 165202–165207.

(51) Slesazeck, S.; Mahne, H.; Wylezich, H.; Wachowiak, A.; Radhakrishnan, J.; Ascoli, A.; Tetzlaff, R.; Mikolajick, T. Physical Model of Threshold Switching in NbO_2 Based Memristors. *RSC Adv.* **2015**, *5*, 102318–102322.

(52) Li, D.; Sharma, A. A.; Gala, D. K.; Shukla, N.; Paik, H.; Datta, S.; Schlom, D. G.; Bain, J. A.; Skowronski, M. Joule Heating-Induced Metal–Insulator Transition in Epitaxial VO_2/TiO_2 Devices. *ACS Appl. Mater. Interfaces* **2016**, *8* (20), 12908–12914.

(53) Ridley, B. K. Specific Negative Reistance in Solids. *Proc. Phys. Soc.* **1963**, *82*, 954-966.

(54) Goodwill, J. M.; Gala, D. K.; Bain, J. A.; Skowronski, M. Switching Dynamics of TaO_x-Based Threshold Switching Devices. *J. Appl. Phys.* **2018**, *123* (11), 115105–115106.

(55) Crespi, L.; Lacaita, A. L.; Boniardi, M.; Varesi, E.; Ghetti, A.; Redaelli, A. Modeling of Atomic Migration Phenomena in Phase Change Memory Devices. *IEEE Int. Memory Workshop* **2015**, 1–4.

(56) Novielli, G.; Ghetti, A.; Varesi, E.; Mauri, A.; Sacco, R. Atomic Migration in Phase Change Materials. IEEE Int. Electron Devices Meet. 2013, pp 22.3.1–22.3.4.

(57) Garg, S. P.; Krishnamurthy, N.; Awasthi, A.; Venkatraman, M. The O-Ta (Oxygen-Tantalum) System. *J. Phase Equilib.* **1996**, *17* (1), 63–77.

(58) Wu, S.; Chan, H. M.; Harmer, M. P. Compositional Tailoring of the Thermal Expansion Coefficient of Tantalum (v) Oxide. *J. Mater. Sci.* **2006**, *41* (3), 689–695.

(59) Gries, U. N.; Schraknepper, H.; Skaja, K.; Gunkel, F.; Hoffmann-Eifert, S.; Waser, R.; De Souza, R. A. A SIMS Study of Cation and Anion Diffusion in Tantalum Oxide. *Phys. Chem. Chem. Phys.* **2017**, *20*, 989–996.

(60) Allnatt, A. R.; Chadwick, A. V. Thermal Diffusion in Crystalline Solids. *Chem. Rev.* **1967**, *67* (6), 681–705.

(61) Muenstermann, R.; Yang, J. J.; Strachan, J. P.; Medeiros-Ribeiro, G.; Dittmann, R.; Waser, R. Morphological and Electrical Changes in TiO_2 Memristive Devices Induced by Electroforming and Switching. *Phys. Status Solidi RRL* **2010**, *4* (1-2), 16–18.

(62) Yang, Y.; Gao, P.; Gaba, S.; Chang, T.; Pan, X. Q.; Lü, W. Observation of Conducting Filament Growth in Nanoscale Resistive Memories. *Nat. Commun.* **2012**, *3*, 732–738.

(63) Yang, Y.; Gao, P.; Li, L.; Pan, X.; Tappertzhofen, S.; Choi, S.; Waser, R.; Valov, I.; Lu, W. D. Electrochemical Dynamics of Nanoscale Metallic Inclusions in Dielectrics. *Nat. Commun.* **2014**, *5*, 1–9.

(64) Sun, H.; Liu, Q.; Li, C.; Long, S.; Lv, H.; Bi, C.; Huo, Z.; Li, L.; Liu, M. Direct Observation of Conversion Between Threshold Switching and Memory Switching Induced by Conductive Filament Morphology. *Adv. Funct. Mater.* **2014**, *24* (36), 5679–5686.

(65) Menzel, S.; Waters, M.; Marchewka, A.; Bottger, U.; Dittmann, R.; Waser, R. Origin of the Ultra-Nonlinear Switching Kinetics in Oxide-Based Resistive Switches. *Adv. Funct. Mater.* **2011**, *21* (23), 4487–4492.

(66) Yalon, E.; Sharma, A. A.; Skowronski, M.; Bain, J. A.; Ritter, D.; Karpov, I. Thermometry of Filamentary RRAM Devices. *IEEE Trans. Electron Devices* **2015**, *62* (9), 2972–2977.